RSC Advances

PAPER

View Article Online
View Journal | View Issue

Cite this: *RSC Adv.*, 2020, **10**, 12304

Lactic-*co*-glycolic acid-coated methylene blue nanoparticles with enhanced antibacterial activity for efficient wound healing†

Xiaomu Xu,‡[ab] Yusheng Hu,‡[bc] Li-peng Zhang,[d] Bo Liu,[b] Yue Yang,[b] Taya Tang,[b] Jijing Tian,[b] Kaisong Peng*[a] and Tianlong Liu *[b]

Received 3rd February 2020
Accepted 13th March 2020

DOI: 10.1039/d0ra01034k

rsc.li/rsc-advances

Effective wound healing has been demonstrated using lactic-*co*-glycolic acid (PLGA)-coated methylene blue nanoparticles (MPNPs) as a novel susceptible agent for photodynamic antibacterial therapy. Compared with methylene blue (MB) solution, MPNPs have a significantly improved antibacterial effect *in vitro* and *in vivo*. The enhanced antibacterial effect is achieved through increased singlet oxygen generation in MPNPs compared to that of MB solution, as a result of the decreased aggregation-induced quenching (ACQ) effect of the MPNPs. The mouse skin infection model experiment proved that MPNP has good antibacterial effects and promotes wound healing.

Bacterial infection is a worldwide public health challenge. Photodynamic therapy (PDT) is a promising antimicrobial therapy and has received increasing attention in recent years for its clinical applications.[1–4] During the process of developing PDTs, various photosensitizers are used.[5,6] Methylene blue (MB) is a traditional photosensitizer, which absorbs energy in light to reach an excited state, and then transfers the energy to a triplet oxygen to induce a singlet state to play a bactericidal role.[7,8] Although MB has wide applications in dentistry and dermatology, the clinical application of MB is limited mainly because of low singlet oxygen yield, toxicity, and low stability. On the other hand, PDT is less likely to evoke drug resistance of the treated bacteria due to its unique antibacterial mechanism.[9,10] However, in order to achieve a satisfactory antibacterial effect, higher laser power is generally required, which also limits the clinical application of PDT.[11] Therefore, it is important to improve the antibacterial efficiency of MB, as well as increase biocompatibility and decrease the laser power required.

Over the past several decades, the rapid development of nanotechnology has shown great potential for the treatment of bacterial infections.[12–14] Given their small size, highly specific surface area, and unique chemical and physical properties, plenty of nanomaterials, such as metal nanoparticles (NPs), metal oxide NPs, carbon nanomaterials and their composites, have been explored as novel antibacterial agents. To date, many nanomaterials have been used in PDT, including TiO_2 nanostructures, ZnO nanocrystals and TAT-TMVCP nanostructure.[15–20] These latest advanced technologies provide novel ideas for the efficient use of MB in biomedical applications.

In the present study, lactic-*co*-glycolic acid (PLGA)-coated MB nanoparticles (MPNPs) were prepared for the treatment of *Escherichia coli* and methicillin-resistant *Staphylococcus aureus* (MRSA) infections. The bacteriostatic effect of MBNPs was evaluated *in vitro* using inhibition zone and minimal inhibitory concentration (MIC) tests. In addition, the therapeutic efficacy of MPNPs against skin infection caused by MRSA was evaluated in mice. MPNPs were prepared using an ultrasonication-assisted coating method described in the ESI.†

The morphology of the prepared MPNPs was characterized by scanning electron microscopy (SEM) and Fourier-transform infrared spectroscopy (FTIR). As shown in Fig. 1, the MPNPs had a uniform morphology with sizes ranging from 100 to 200 nm (Fig. 1A). The dynamic light scattering (DLS) spectrum showed that ultrafine MPNPs with an average hydrodynamic diameter of 247.7 nm and polydispersity index (PDI) of 0.153 were formed (Fig. S1 and S2†). Fig. S3† shows a zeta of −0.319 mV which is characteristic of negatively charged MPNPs. The TEM image of MPNPs clearly shows that the MPNP thickness was roughly 200 nm, suggesting that the NPs existed (Fig. S4†). Compared with MB, new absorption bands appeared

[a]*Laboratory of Aquatic Health and Public Health, College of Animal Science and Technology, Anhui Agricultural University, Hefei 230036, China. E-mail: kaisongpeng@ahau.edu.cn*

[b]*Laboratory of Veterinary Pathology and Nanopathology, College of Veterinary Medicine, China Agricultural University, No. 2 West Road Yuanmingyuan, Beijing 100193, P. R. China*

[c]*College of Biological Sciences, China Agricultural University, No. 2 West Road Yuanmingyuan, Beijing 100193, P. R. China*

[d]*Key Laboratory of Photochemical Conversion and Optoelectronic Materials, Technical Institute of Physics and Chemistry, Chinese Academy of Sciences, 29 Zhongguancun East Road, Haidian District, Beijing, 100190, China*

† Electronic supplementary information (ESI) available. See DOI: 10.1039/d0ra01034k

‡ These authors contributed equally.

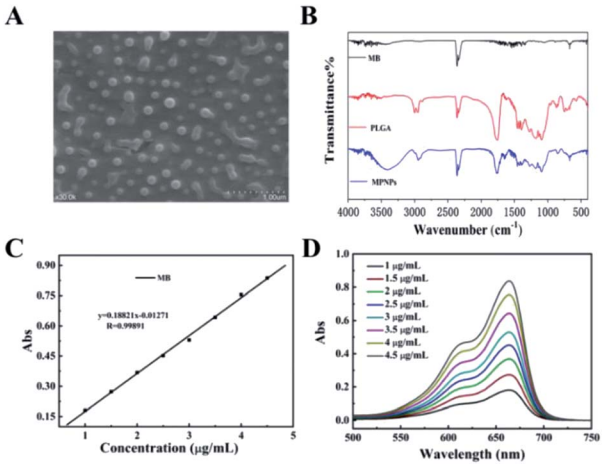

Fig. 1 (A) MPNP SEM images. (B) FTIR spectra of methylene blue (MB)-, lactic-*co*-glycolic acid (PLGA)-, and PLGA-coated MB nanoparticles (MPNPs). (C) Standard curve line of MB (663.5 nm) (D) ultraviolet-visible absorption spectra of MB.

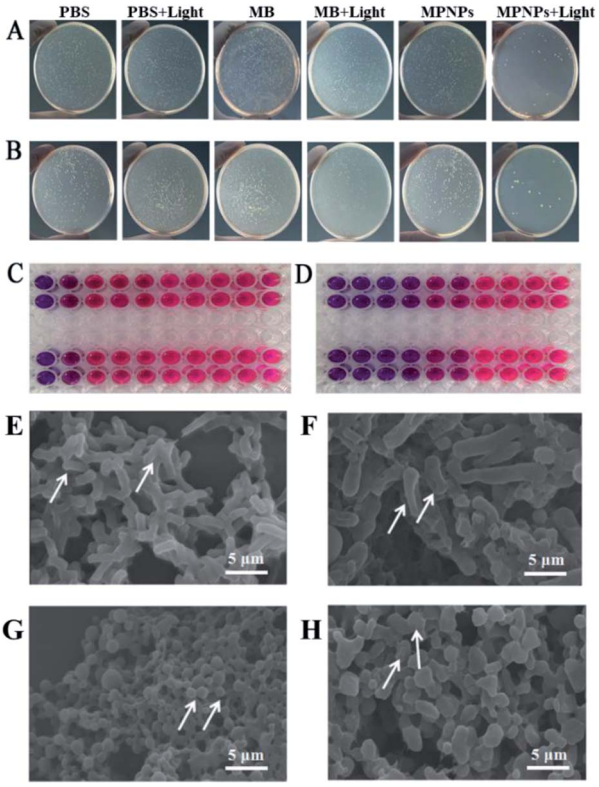

Fig. 2 Photographs of bacterial colonies formed on LB agar plates of (A) *E. coli* and (B) *S. aureus* (PBS, PBS + light, MB, MB + light, MPNPs, and MPNPs + light). (C) Image for MIC of MB with 660 nm laser against *E. coli* and MRSA. (D) Image for MIC of MPNPs with 660 nm laser against *E. coli* and MRSA. (E) SEM images of *E. coli* in PBS, (F) SEM images of *E. coli* treated with MPNPs and laser, (G) SEM images of MRSA in PBS, (H) SEM images of MRSA treated with MPNPs and laser.

at 2300, 1750, and 700 cm^{-1} on the FTIR spectrum of MPNPs (Fig. 1B). The absorption band at 2300 cm^{-1} originated from the stretching mode of the CN chains. The absorption band at 1750 cm^{-1} belonged to the bending vibration of the benzene ring C–C skeleton of MB, and the absorption band at 700 cm^{-1} belonged to the Cl^{-1} absorption peak. This result indicates that MB was successfully coated with PLGA. The UV-Vis absorption spectra of MPNPs shown in Fig. 1C and D indicates that the MBNPs exhibited broad absorption from the UV to NIR region at different concentrations (1, 1.5, 2, 2.5, 3, 3.5, 4, 4.5, and 5 μg mL^{-1}). These results show a maximum absorbance at 663.5 nm which is the characteristic wavelength for MB.

The antibacterial property of MPNPs *in vitro* against MRSA and *E. coli* was evaluated by an agarose diffusion assay. Series concentrations of MPNPs are set as 200, 100, 50, 25, 12.5 μg mL^{-1}. Fig. 2A shows the satisfactory antibacterial effect of MPNPs (100 μg mL^{-1}) against *E. coli*. Compared with that in other groups, MPNPs with 660 nm laser irradiation for 5 min (MPNPs + light) could inhibit the growth of *E. coli in vitro* at a restrained growth rate of 99.99%. The same results were obtained from evaluation of MPNPs against MRSA (Fig. 2B). Table S1† shows the restrain rate of different groups against *E. coli* and MRSA. Treatment of *E. coli* with MPNPs that received laser irradiation for 5 min caused a 99.99% restrained growth rate, which was significantly higher than treatment with MB + light, MPNPs or laser irradiation (80%, 35% and 25%, respectively). For MRSA, the growth restrain rate after treatment with MPNPs plus laser was 99.97%, which was significantly higher than those for the other treatment groups (MB 27%, MB + light 75%, MPNPs 30%, laser 40%). The MIC test results showed that MPNPs plus laser irradiation had a lower MIC than the MPNP alone group (Fig. 2C and D). A summary of the MIC results is listed in the ESI.† In brief, bacteria (100 μL) were treated with different concentrations of MPNPs (3.125, 6.25, 12.5, 25, 50, 100, and 200 μg mL^{-1}, 100 μL) with or without 660 nm laser irradiation and incubated at 37 °C for 16 hours. Resazurin solution was added to the plates, which were then incubated for an additional 4 hours. The cells were then treated with laser irradiation at a power density of 1.0 W cm^{-2} for 5 min. The solution in the wells with values higher than the MIC remained blue whereas those with values less than the MIC became red. Fig. 2C shows that the MIC of MPNPs against *E. coli* (upper line) and MRSA (lower line) was 100 μg mL^{-1}. The MIC of MPNPs + light was 25 μg mL^{-1} against *E. coli* (upper line) and MRSA (lower line) (Fig. 2D). These results indicate efficient antibacterial activity of MPNPs under 660 nm irradiation against clinically common pathogenic bacteria *in vitro*.

Ultrastructural SEM observations of *E. coli* and MRSA that received MPNP and 660 nm laser irradiation treatment provide further support for the conclusion. Fig. 2E and G show SEM images of *E. coli* and MRSA for the negative control group. In the negative control group, *E. coli* appeared rod-shaped with a smooth surface. Conversely, bacterial cells treated with MPNPs and laser irradiation have significant surface wrinkling indicating dramatic damage of the bacterial cell wall (Fig. 2F). In the negative control group, MRSA appeared circular and the cell surface was intact. MRSA cells treated with MPNPs plus laser irradiation showed ultrastructural changes including adherence to one another, various sizes, and an overflow of

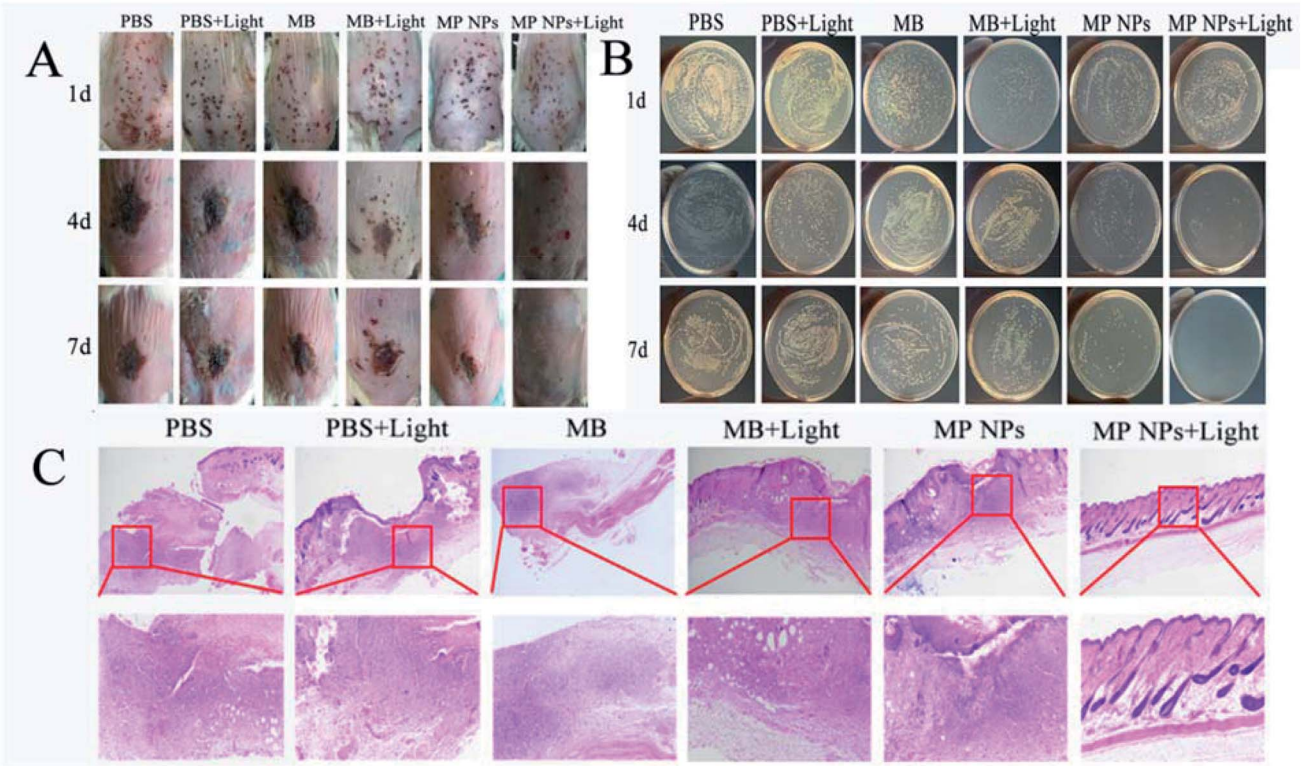

Fig. 3 (A) Photographs of infected wounds in mice at different timepoints after various treatments: PBS, PBS + light, MB, MB + light, MPNPs, and MPNPs + light. (B) Photographs of bacterial colonies formation on LB agar plates from the infected wounds after different treatments. (C) Photomicrographs of tissue sections of MRSA infected wounds in mice treated with PBS, PBS + light, MB, MB + light, MPNPs, and MPNPs + light after H&E staining. The scale bar is 500 μm.

cellular contents (Fig. 2H). These results indicate that MPNPs with laser irradiation induce damage of bacteria.

Mice with MRSA skin infection were used for *in vivo* experimentation. The mice were divided into six groups: PBS, PBS + light, MB, MB + light, MPNPs, and MPNPs + light. For the light-treatment groups, the infected mice were irradiated with a 660 nm laser at a power density of 1 W cm^{-2} for 5 min. As shown in Fig. 3A, the images of the wound skin on different days after various treatments indicated that MPNPs + light promote wound healing to a greater extent than the other treatments. At 4 days post-treatment, the wound on the back skin of mice in the MPNPs + light group began to close. Wounds of mice in the other treatment groups were black and began to form scars. At 7 days post-treatment, the wounds of mice in the MPNPs + light group had healed completely. The wound areas of mice in the other groups were smaller at day 4, but the black scars remained.

At days 1, 4, and 7 post-treatment, MRSA cell counting was performed for all groups. Fig. 3B shows the colony forming unit (CFU) results of different groups at these three time points. At day 4 and 7 post-treatment, the CFUs of the PBS + light or MB groups were similar to that of the PBS group, while the CFUs of live bacteria in wounds treated with MB + light and MPNPs were reduced. In contrast, treatment with MPNPs with laser irradiation can inhibit the growth of the bacteria significantly, especially at day 7 post-treatment indicated by the absence of bacteria present in the wound site (Fig. S5†). The relative wound area in MPNPs + Light group decreased to 36.93% and 0% on day 4 and day 7 (Fig. S7†).

Further histological examination was performed of the wound after different treatments. In Fig. 3C, hematoxylin–eosin (H&E) staining images show that the skin remained an intact with no apparent cell infiltration in the MPNPs plus laser group. In the other groups, these mice showed an incomplete epidermal structure, severe tissue edema, as well as massive leukocytes infiltration into the wound and surrounding tissue (Fig. 3C). Moreover, the presence of hair follicles also indicates better healing of the wounds in the MPNPs plus laser group. These results suggest enhanced recovery of mice that received MPNPs and laser treatment compared to that of mice in the other treatment groups. In order to evaluate the biocompatible of MPNPs, the cytotoxicity of the prepared NPs were examined using MTT methods. After 24 hours of incubation with MPNPs, there was no observable change to the relative viability of 4T1 cells even at a concentration of up to 200 μg mL^{-1}, indicating low cytotoxicity of the tested NPs (Fig. S6†). Actually, mice of all groups were measure for pathological studies *in vivo*. No obvious change were observed in the major organs of all groups shown in (Fig. S8†).

In the present study, compared with MB plus laser irradiation treatment, MPNPs plus laser exhibited excellent antibacterial effects against *E. coli* and MRSA. The hypothetical

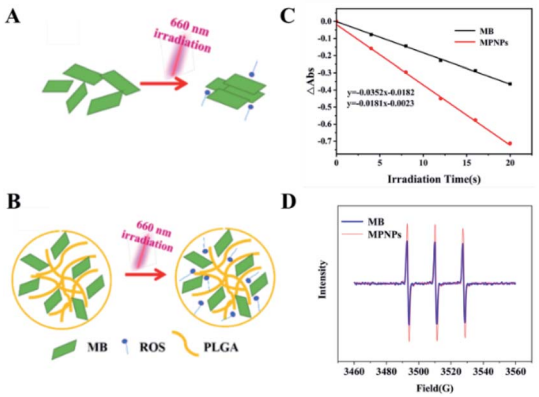

Fig. 4 (A) Schematic of singlet oxygen aggregation-caused quenching (ACQ) effect of MB. (B) PLGA reduces the ACQ effect of MPNPs. (C) ABDA absorption curve of MB and MPNPs in water. (D) EPR spectrum of MB and MPNPs.

mechanism is that more $^1O_2$ is generated by MPNPs than MB under 660 nm irradiation as a result of the reduced stacking effect of singlet oxygen produced by MPNPs. As shown in Fig. 4A, singlet oxygen produced by MB will be quenched due to the aggregation-caused quenching (ACQ) effect. The singlet oxygen produced by MPNPs will exist longer because the PLGA molecule affect the aggregation state of MB reducing the ACQ effect (Fig. 4B). The significant decline of ABDA absorptions demonstrated the good $^1O_2$ generation abilities of MPNPs in water (Fig. 4C). Electron paramagnetic resonance (EPR) analysis results also show an increase of $^1O_2$ generation of MPNPs compared to MB under 660 nm laser irradiation (Fig. 4D). These results support the hypothetical mechanism of MPNPs.

In summary, MPNPs have a remarkable antibacterial effect compared to MB against *E. coli* and MRSA *in vitro* and *in vivo*. In order to explore the mechanism of action of MPNPs, the condition of cell membranes and singlet oxygen release were tested. We propose that reduction in the ACG effect of MB is caused by the PLGA molecule. Instead of free MB, MPNPs enhanced the lifespan of singlet oxygen produced by MB and the chance of them contacting the cell membranes. Using this strategy, other agents may be coated with PLGA to enhance their antimicrobial effects in future clinical applications.

Ethical statement

Experimentation with animals was governed by the Regulations of Experimental Animals of Beijing Authority and approved by the Animal Ethics Committee of the Peiking University. ICR mice (provided by Vital River Laboratory Animal Technology Co. Ltd., Beijing), aged 6–8 weeks, were used in the experiments. Mice were raised in independent ventilated cages and received pathogen-free food and water.

Conflicts of interest

There are no conflicts to declare.

Acknowledgements

The authors acknowledge financial supported by National Natural Science Foundation of China (31802237), Beijing Natural Science Foundation (6202017) and Young Teachers Innovation Project of China Agricultural University (2018QC142).

Notes and references

1 Z. Wang, K. Dong, Z. Liu, Y. Zhang, Z. Chen, H. Sun, J. Ren and X. Qu, *Biomaterials*, 2017, **113**, 145.
2 L. Sun, W. Jiang, H. Zhang, Y. Guo, W. Chen, Y. Jin, H. Chen, K. Du, H. Dai, J. Ji and B. Wang, *ACS Appl. Mater. Interfaces*, 2019, **11**, 22302.
3 S. Jeong, J. Lee, B. N. Im, H. Park and K. Na, *Biomaterials*, 2017, **141**, 243–250.
4 C. Hu, F. Zhang, Q. Kong, Y. Lu, B. Zhang, C. Wu, R. Luo and Y. Wang, *Biomacromolecules*, 2019, **20**, 4581–4592.
5 X. Miao, W. Hu, T. He, H. Tao, Q. Wang, R. Chen, L. Jin, H. Zhao, X. Lu, Q. Fan and W. Huang, *Chem. Sci.*, 2019, **10**, 3096–3102.
6 Q. Liu, J. Wang, S. Li, G. Li, Q. Chen and Z. Hong, *J. Pharmaceut. Sci.*, 2019, **108**, 2102–2111.
7 R. López-Igual, J. Bernal-Bayard, A. Rodríguez-Patón, J.-M. Ghigo and D. Mazel, *Nat. Biotechnol.*, 2019, 755–760.
8 T. T. Yao, J. Wang, Y. F. Xue, W. J. Yu, Q. Gao, L. Ferreira, K. F. Ren and J. Ji, *J. Mater. Chem. B*, 2019, **7**, 5089–5095.
9 T. W. Wong, S. Z. Liao, W. C. Ko, C. J. Wu, S. B. Wu, Y. C. Chuang and I. H. Huang, *J. Clin. Med.*, 2019, **8**, 1028.
10 M. Jia, B. Mai, S. Liu, Z. Li, Q. Liu and P. Wang, *Photodiagnosis Photodyn. Ther.*, 2019, **28**, 80–87.
11 X. Li, N. Kwon, T. Guo, Z. Liu and J. Yoon, *Angew. Chem., Int. Ed.*, 2018, **57**, 11522.
12 M. A. M. Jahromi, P. S. Zangabad, S. M. M. Basri, K. S. Zangabad, A. Ghamarypour, A. R. Aref, M. Karimi and M. R. Hamblin, *Adv. Drug Delivery Rev.*, 2018, **123**, 33.
13 H. B. Cheng, X. Li, N. Kwon, Y. Fang, G. Baek and J. Yoon, *Chem. Commun.*, 2019, **55**, 12316–12319.
14 F. Xu, Y. Zhao, M. Hu, P. Zhang, N. Kong, R. Liu, C. Liu and S. K. Choi, *Chem. Commun.*, 2018, **54**, 9525–9528.
15 T. V. Torbati and V. Javanbakht, *Colloids Surf. B Biointerfaces*, 2019, 110652.
16 W. Ma, L. Li, X. Lin, Y. Wang, X. Ren and T. S. Huang, *ACS Appl. Mater. Interfaces*, 2019, **11**, 31411–31420.
17 Z. M. Markovic, M. Kovacova, P. Humpolicek, M. D. Budimir, J. Vajdak, P. Kubat, M. Micusik, H. Svajdlenkova, M. Danko, Z. Capakova, M. Lehocky, B. M. Todorovic Markovic and Z. Spitalsky, *Photodiagnosis Photodyn. Ther.*, 2019, **26**, 342–349.
18 S. Gao, X. Yan, G. Xie, M. Zhu, X. Ju, P. J. Stang, Y. Tian and Z. Niu, *Proc. Natl. Acad. Sci. U. S. A.*, 2019, **116**, 23437–23443.
19 J. Sun, S. Kormakov, Y. Liu, Y. Huang, D. Wu and Z. Yang, *Molecules*, 2018, **23**, 1704.
20 A. F. Silva, A. Borges, E. Giaouris, J. M. Graton Mikcha and M. Simoes, *Crit. Rev. Microbiol.*, 2018, **44**, 667.